By Emily A. Smith* and Robert M. Corn
Department of Chemistry
University of Wisconsin
Madison, Wisconsin 53706

Surface Plasmon Resonance Imaging as a Tool to Monitor Biomolecular Interactions in an Array Based Format

INTRODUCTION

Nearly all processes within a living organism are driven by biomolecular interactions. In order to fully understand the role of a newly discovered gene or protein within a biological system it is necessary to know what molecules it interacts with and what the possible outcomes of these interactions are. One consequence of biological diversity is that there are many potential interacting partners in living systems (e.g., DNA, RNA peptides, proteins, lipids, and carbohydrates) with a broad range of chemical properties. The mechanisms through which these partners interact are as diverse as the interacting partners themselves: they may interact very weakly, form a strong chemical bond, have cooperative or multiple binding interactions, create an entity with enzymatic activity, etc.

Methods that are capable of rapidly screening diverse sets of biomolecular interactions are necessary in order to decipher the wealth of information that exists for the genomes and proteomes of many organisms. One way to accomplish this screening is to attach a set of biomolecules (arbitrarily defined as probes) to a surface in an array format and then expose the array to another set of biomolecules (arbitrarily defined as targets) that are in solution. The use of an array format to study biomolecular interactions has several benefits over solution-based methods: the use of small analyte volumes, the ability to perform parallel screening of multiple interactions, and the ability to provide straightforward and rapid response read-outs. Numerous detection methods have been used to study biomolecular interactions on surfaces, including total internal reflection fluorescence,[1] wave guides,[2,3] ellipsometry,[4,5] atomic force microscopy,[6,7] and surface plasmon resonance (SPR).[8–10] In this article we will describe the use of SPR imaging as a method for screening biomolecular interactions.

Surface plasmon resonance is a

* Current Address: Department of Chemistry and Biochemistry, University of Delaware, Newark, Delaware 19716.

sensitive, label-free technique that can provide real-time data on adsorption and/or desorption events that occur at a metal/dielectric interface. There are several instrumental formats that can be used in SPR experiments; these can be roughly categorized into three types of measurements: scanning angle SPR,[11–14] scanning wavelength SPR,[15] and SPR imaging.[9,16–22] For all SPR formats, the reflectivity of light incident on a metal/dielectric interface is monitored and correlated to changes in the local index of refraction of the dielectric layer adjacent to the metal film. The most widely used format for an SPR experiment is the scanning angle technique, in which the reflectivity of monochromatic incident light upon a metal film is monitored as a function of the incident angle. The popularity of the scanning angle technique can be partially attributed to the existence of commercially available instrumentation from Biacore,[23] which has made it possible to use SPR as a detection method for many applications, including basic life science research, drug discovery, environmental monitoring, and process analysis. Both the scanning angle and scanning wavelength measurements typically provide only one or a few data points at a time. In contrast, SPR imaging measurements, sometimes called SPR microscopy, use the changes in reflectivity from a gold thin film that occur upon adsorption to generate difference images to simultaneously monitor tens, hundreds, or more interactions in a parallel manner.

The high-throughput capabilities of SPR imaging have made it an attractive tool for screening biomolecular interactions. For example, SPR imaging has been used in an array format to study the hybridization of DNA and RNA to nucleic acid arrays fabricated on gold films.[9,20,24,25] Shown in Fig. 1A is an example of an SPR difference image of a two-component DNA array. The difference image was obtained by subtracting the images taken before and after exposing the array to a 16-mer that was complementary to the immobilized sequence 1, which was patterned on the surface as shown in Fig. 1B. A change in the reflected light intensity was observed only where sequence 1 was immobilized on the array, demonstrating the specific hybridization of the target to the complementary immobilized sequence. Shown in Fig. 1C is a plot of a line profile that was acquired from the SPR image (indicated by the black line in Fig. 1A). The plot shows that the hybridization of the 16-mer complementary sequence corresponds to less than a one percent change in the reflected light intensity and that there is no change in the reflected light intensity for the non-complementary sequence. DNA arrays have also been used in conjunction with SPR imaging to monitor RNA hybridization,[9] for DNA word design in computational algorithms,[26] for single base mismatch detection (discussed below), and to monitor hairpin formation in DNA monolayers.[27]

The next section of this article will provide a brief background to the SPR imaging technique, including an introduction to surface plasmons. Following this background section, the remainder of the article will highlight SPR imaging instrumentation, array fabrication techniques, and the ability to obtain quantitative data with SPR imaging. A few examples of the use of SPR imaging for the study of biomolecular interactions will also be presented.

SURFACE PLASMON RESONANCE THEORY

Surface plasmons (SPs) are oscillations of free electrons that propagate along the surface of a metal when it is in contact with a dielectric interface. Surface plasmons can have a range of energies that depend on the complex dielectric function of the metal (ε_m) and the dielectric function of the adjacent medium (ε_d), as shown by the following equation:

$$k_{sp} = \frac{\omega}{c}\sqrt{\frac{\varepsilon_m \varepsilon_d}{\varepsilon_m + \varepsilon_d}} \qquad (1)$$

where k_{sp} is the wave vector of the SP, ω/c is the wave vector in a vacuum, and the dielectric constant is the square of the index of refraction.[28] One condition for the generation of SPs is that ε_m and ε_d are of opposite sign, and thus SPs will not be generated for all systems. In addition, ε_m and ε_d are wavelength dependent, and certain regions of the electromagnetic spectrum may be required to generate SPs. One common system used in SPR experiments is a gold film in contact with a water interface. Gold has a negative dielectric function in the IR and visible regions of the electromagnetic spectrum, whereas water has a positive dielectric function.[29]

Surface plasmons can be directly excited by electrons; however, they can not be excited directly by light because they have a longer wave vector than light waves of the same energy ($k_{light} = \omega/c$). The wave vector of a photon must be increased to convert the photon into SPs. This can be accomplished with the use of either a prism or a grating coupler.[28] For example, SPs can be excited under conditions of attenuated total reflection (ATR) using a prism/metal film/dielectric layer (designated the Kretschmann configuration)[30] and *p*-polarized incident light that has its electric component in the plane of incidence. Shown in Fig. 2 is a schematic diagram of a Kretschmann configuration sample setup that has been used for the study of biomolecular interactions with SPR imaging. The setup consists of a high-index-of-refraction glass prism, a 45 nm Au film (with a 1 nm Cr underlayer), a 2 nm self-assembled monolayer, a 5 nm sensing layer where adsorption of the target molecule occurs, and a bulk water layer.

The equation for the surface component of a photon's wave vector under conditions of ATR becomes:

$$k_{ATR} = \frac{\omega}{c} \sin\theta \sqrt{\varepsilon_p} \qquad (2)$$

where ε_p is the dielectric constant of the prism, and θ is the angle of incidence of the light on the metal film.[28] SPs will be generated in the

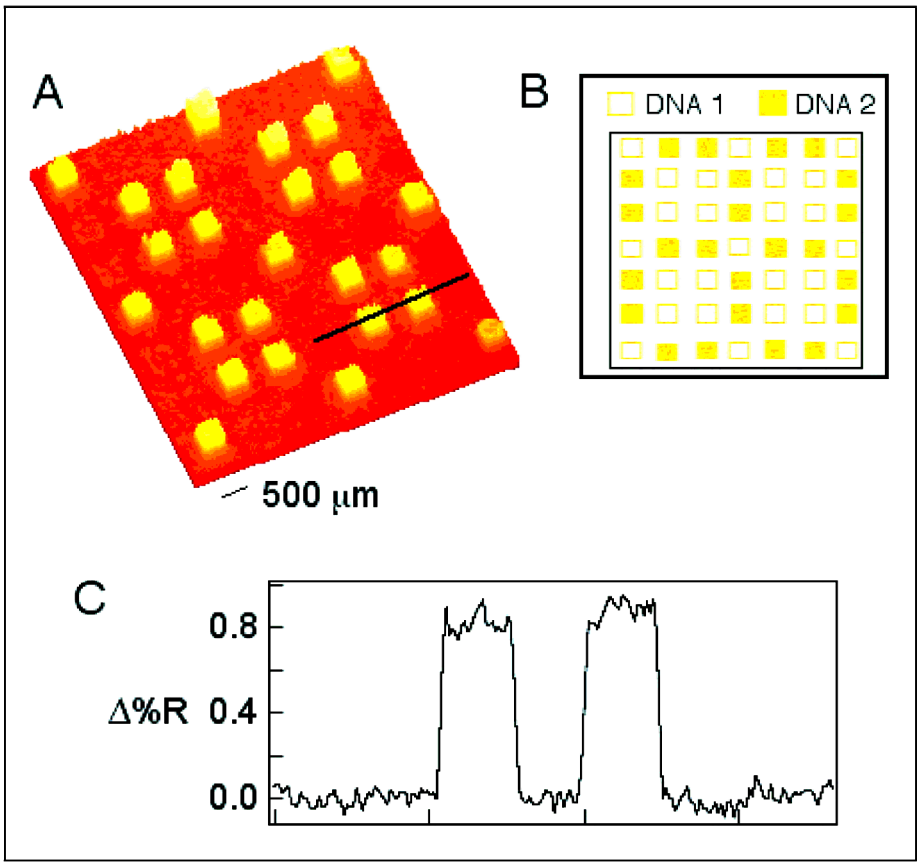

Fig. 1. **(A)** *SPR difference image of a two-component DNA array showing the hybridization of a sequence complementary to immobilized sequence 1;* **(B)** *schematic diagram showing the pattern of the immobilized DNA sequences for the SPR image shown in A; and* **(C)** *line profile plotted as the change in percent reflectivity obtained from the area indicated by the black line in the SPR image.*

metal film at angles where the photon's wave vector equals the SP's wave vector. The excitation of SPs corresponds to an attenuation of the reflected light intensity as the incoming light generates SPs. The angle where there is a complete attenuation of the reflected light corresponds to the complete conversion of the incoming light and is referred to as the surface plasmon angle.

Fresnel equations can be used to predict the reflectivity and phase shift when incident light impinges on an interface containing two or more phases.[31] These calculations assume that each phase is homogenous and parallel, and they require knowledge of the complex index of refraction of each of the phases, which are dependent on the wavelength of the incident light. The reflection coefficient for *p*-polarized incident light is given by the formula:

$$r_p = \frac{E^r}{E^t} \qquad (3)$$

where E^r is the electric field component in the plane of incidence of the light reflected from the interface, and E^t is the electric field component in the plane of incidence of the light transmitted through the interface. The light reflected from the interface can be calculated using the formula:

$$R_p = |r_p|^2 \qquad (4)$$

For multiphase systems, these calculations require matrix operations. Computer programs have been developed to calculate the reflected light intensity for multiphase systems where one or more of the phases are a material with a complex index of refraction (i.e., a metal film).[23] Shown in Fig. 3 are the results of 5-phase Fresnel calculations used to simulate scanning angle SPR reflectivity curves from the sample setup depicted in Fig. 2. The reflectivity of light is plotted versus the angle of incidence for two films with sensing layers that have an index of refraction (n_f) of 1.40 or 1.46. An increase in the index of refraction of the sensing layer simulates adsorption onto the metal film. Conditions of ATR are met at angles greater than the critical angle, which occurs near 50.6 degrees. As mentioned previously, the surface plasmon angle corresponds to the angle where there is a near complete attenuation of the reflected light. The position of the surface plasmon angle is dependent on the index of refraction of the

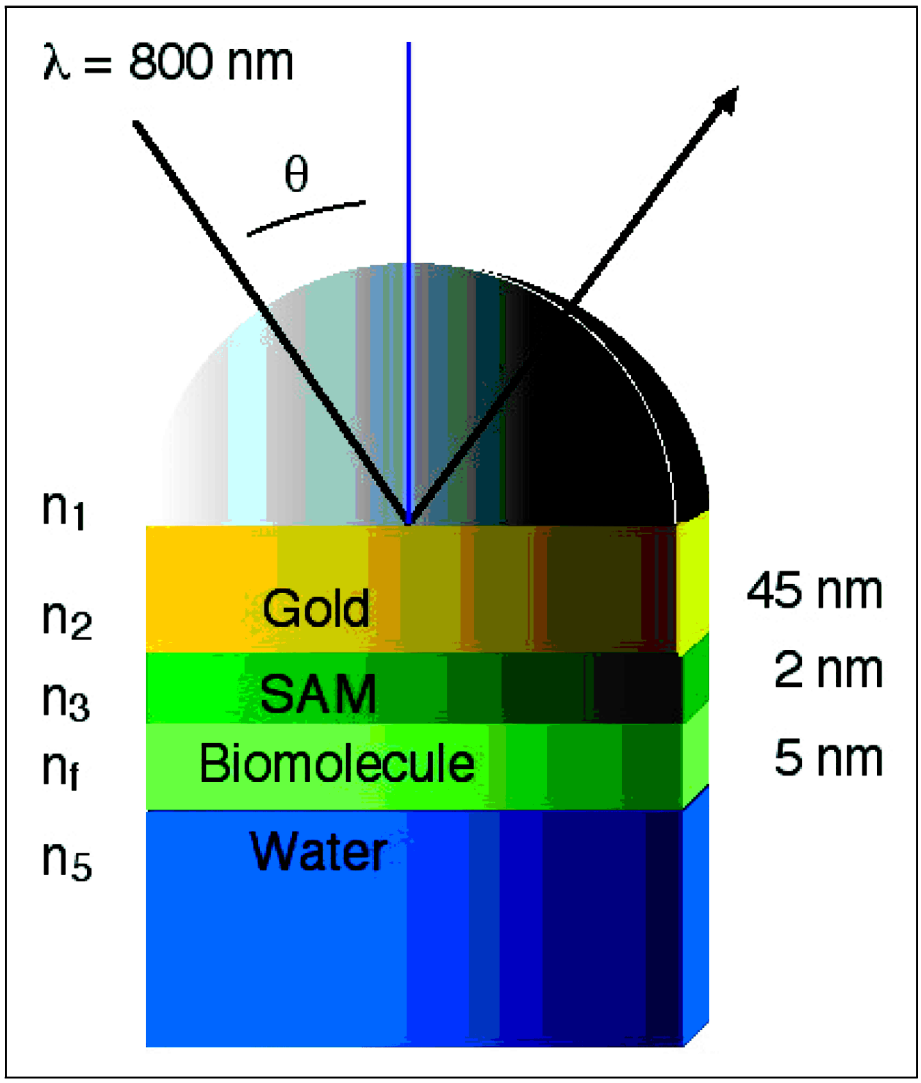

Fig. 2. Diagram showing a sample setup used to monitor biomolecular interactions with SPR imaging. The 5 phases are a high-index-of-refraction glass prism (n_1 = 1.712), a 45-nm-thick gold film (n_2 = 0.1451 + 4.8725), a 2 nm self-assembled monolayer (n_3 = 1.45), a 5 nm sensing layer where adsorption occurs (n_f), and a bulk water layer (n_5). Adsorption of biomolecules to the sensing layer increases the value of n_f.

sensing layer. An expanded view of the region encompassing the surface plasmon angles for both films is shown in Fig. 3 (right inset).

Surface plasmons have a maximum intensity in the metal film, and they decay exponentially in a perpendicular direction from the surface in both the metal and the dielectric layer.[28] The decay length of the SPs is dependent on the wavelength of the incident light and on the dielectric constants of both layers. For a gold film, a typical decay length is on the order of a few hundred nanometers into the dielectric layer for excitation with visible light. This means that SPR is a surface sensitive technique and that measurements can be made even when a large excess of analyte is present in solution. Any species that is farther from the metal film than the SP decay length will not effect the generation of SPs.

The propagation length of SPs is the distance where its electric field intensity in the metal film drops to a value of 1/e and is determined by ε_m, ε_d, and the wavelength of the incident light.[28] The SP propagation length determines the lateral resolution in SPR imaging. In order to resolve two features, they must be separated by a minimum distance corresponding to the propagation length of the SP. Longer SP propagation lengths correlate to a lower lateral resolution, and higher lateral resolution can be achieved using shorter wavelength light.

The sensitivity in SPR imaging, the ability to detect small changes in n_f, is also affected by the wavelength of the incident light. Incident light of longer wavelengths produces sharper SPR curves (with narrow widths at 50% reflectivity), and incident light of shorter wavelengths produces

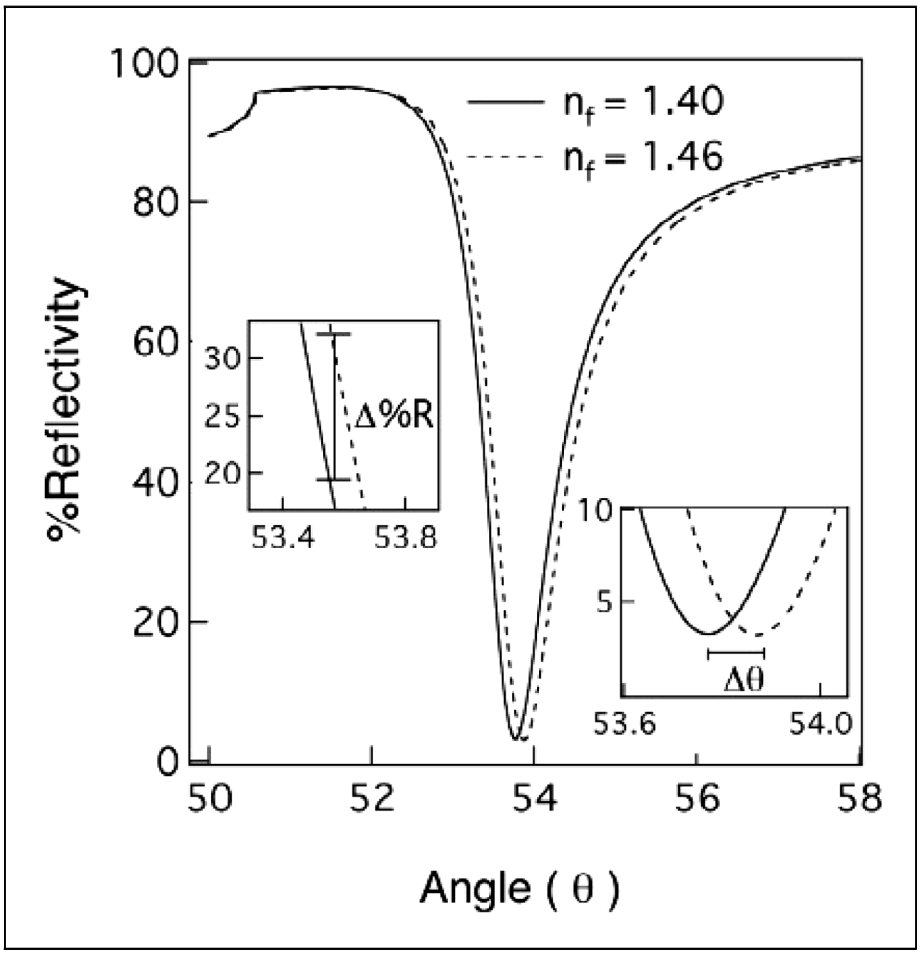

Fig. 3. Graph showing the scanning angle SPR reflectivity curves that were obtained from 5-phase Fresnel calculations for the system shown in Fig. 2. The index of refraction of the sensing layer (n_f) was 1.40 (solid line) or 1.46 (dotted line). The figure inset at right shows an expanded view of the region near the plasmon angles. The location of the plasmon angle shifts to higher angles for the n_f = 1.46 film relative to the n_f = 1.40 film. The figure inset at left shows an expanded view around the optimal angle for performing SPR imaging experiments with this system. At the optimal angle the largest shift in %R is observed for these two films.

broad SPR curves (with large widths at 50% reflectivity).[32] Sharper SPR curves produced by longer wavelength incident light yield larger changes in reflectivity for given changes in n_f than do broad curves produced by incident light with shorter wavelengths. This means that there is a trade-off between lateral resolution and sensitivity. The use of longer wavelength light provides higher sensitivity, but lower lateral resolution. The use of shorter wavelength light provides a higher lateral resolution, but lower sensitivity.[33,34]

SURFACE PLASMON RESONANCE IMAGING

Surface Plasmon Resonance Imaging Instrumentation. Surface plasmon resonance imaging is a fixed angle experiment where the spatial changes in reflected light are measured across a substrate. The theoretical curves generated for a scanning angle SPR experiment can be used to understand the basis of the contrast observed in an imaging experiment. The left inset in Fig. 3 shows an expanded region around an incident angle of 53.5 degrees. A slice through the X-axis simulates a constant angle experiment. At 53.5 degrees, less light is reflected from the n_f = 1.40 film than the n_f = 1.46 film. If a surface were patterned to contain regions with both films, more light would be reflected from the regions with n_f = 1.46 than regions containing the n_f = 1.40 film at an angle of 53.5 degrees, and it would be possible to distinguish between the two films in an SPR image.

The basic components in a typical SPR imaging instrument are shown in Fig. 4. These are a collimated white light source, a polarizer, the sample stage, collection optics, and a charge-coupled device (CCD) connected to a CPU for image collection and processing. The use of a collimated white light source is preferred over the use of laser excitation due to interference fringes that result in the SPR image when laser excitation is utilized. The polarizer is used to select *p*-polarized light, and the col-

lection optics consist of a narrow band pass filter, typically centered in the near-infrared region, that is used to select the excitation wavelength for the experiment. The sample is located on a rotation stage in order to control the incident angle of light and consists of a prism, a substrate onto which a Au film is deposited, and a flow cell.

Attachment Chemistry and Array Fabrication. Surface plasmon resonance imaging is performed on a noble metal film; therefore, strategies for attaching probe molecules to these films are critical to the success of an SPR imaging experiment. Numerous immobilization strategies exist. These can generally be categorized into three routes: (1) a thiol-modified probe molecule can be reacted directly with a gold film to form a gold–thiolate bond;[35] (2) a polymer layer, such as dextran or polylysine, can be first formed on the gold surface, and the probe molecule can be immobilized onto the polymer layer;[36] and (3) a self-assembled alkanethiol monolayer (SAM) containing a ω-terminated functional group can be formed on the gold film, which is used to immobilize a molecule (a ''linker'') that is capable of reacting with the probe molecule.[37–41]

There are drawbacks to the first and second immobilization schemes. Many biomolecules will non-specifically adsorb to a gold film, and a large portion of the probes may not be biologically active if they are directly attached to the gold film. Surfaces fabricated using the second immobilization strategy may not be robust and polymer layers can be a problem when studying kinetics of adsorption.

Several characteristics of the third immobilization scheme make it suitable for use with SPR imaging. Generally, the surfaces that result from this immobilization strategy are stable and can be used for several assay cycles. Using this immobilization strategy provides a way to control the surface density of the probe molecule. This is important for two reasons: (1) the surface density of the probe can affect the amount of target that binds to the surface, and therefore, the amount of signal that is detected; and (2) varying the probe density can be used as a tool to study the interactions of targets that bind to the probes through multivalent interactions (an example of this is the use of SPR imaging to study carbohydrate–protein interactions). Finally, this strategy provides a way to control the resulting surface properties (i.e., hydrophilic, hydrophobic, charged).[42–47] This is important since everything that adsorbs to the gold surface will produce an SPR signal; it is necessary to control the surface properties so that only the desired target molecules interact with the surface.

In addition to immobilizing probe molecules to a gold film, the film must be patterned so that several probes are immobilized at discrete locations on the substrate. There are several methods that have been used to pattern gold films. UV photopatterning,[17,41] polydimethylsiloxane (PDMS) microchannels,[48] microcontact printing,[49] and robotic spotting[50] have been used in conjunction with SPR imaging. The array shown in Fig. 1 was fabricated using the UV photopatterning method, in which a quartz mask is used to selectively expose an alkanethiol-modified gold surface to UV light. At locations where the UV light shines on the surface, the alkanethiol is removed, generating bare gold patches that serve as a platform for generating the array elements. Both the UV photopatterning and PDMS microchannel array fabrication strategies will be discussed later in this article in conjunction with specific examples of the use of SPR imaging to study biomolecular interactions.

Quantitation of Results Generated with Surface Plasmon Resonance Imaging. In addition to the ability to detect interacting partners with SPR imaging, it is desirable to obtain quantitative information about these interactions. Quantitative data can be obtained from SPR measurements by assuming that molecules adsorbing to or desorbing from the metal film correlate to changes in the index of refraction of the dielectric layer and that changes in the index of refraction correlate to changes in the reflectivity of the incident light. In order to obtain quantitative data with SPR imaging, it is necessary to know over what regions there is a linear relationship between the change in the reflected light intensity ($\Delta\%R$) and the change in the index of refraction of the sensing layer (Δn_f). A series of 5-phase Fresnel calculations of the system shown in Fig. 2 can be used to determine this.[9] The first calculation is performed with an n_f value of 1.4. Each successive calculation increments the n_f value by 0.002 index of refraction units. Figure 5 shows the results from these calculations plotted as the absolute value of $\Delta\%R$ for the indicated Δn_f. These calculations were performed for an excitation wavelength of 794 nm, and the results at three angles along the SPR curve are shown (the location of the angles along the SPR curve are shown in the figure inset). The dotted lines in Fig. 5 show a linear relationship between $\Delta\%R$ and Δn_f. At an angle of 53.52 degrees, the greatest contrast is predicted, as determined by the magnitude of $\Delta\%R$. The smallest deviation from linearity is also observed at 53.52 degrees. A small change in the incident angle of 0.04 degrees does not significantly affect the overall signal or the amount of deviation that occurs. This is not the case for angles greater than 0.1 degrees from the optimal angle of 53.52 degrees (not shown in Fig. 5). At angles further than 0.1 degrees from the optimal angle there is a smaller change in the percent of reflected light, and these signals deviate from a linear relationship at large n_f values. While the data is fairly linear for an angle higher than the surface plasmon angle (54.12), the overall contrast that would be observed is much smaller than for angles to the left of the surface plasmon angle. This is a result of the SPR curve not being symmetric about the surface plasmon angle (see Fig. 3).

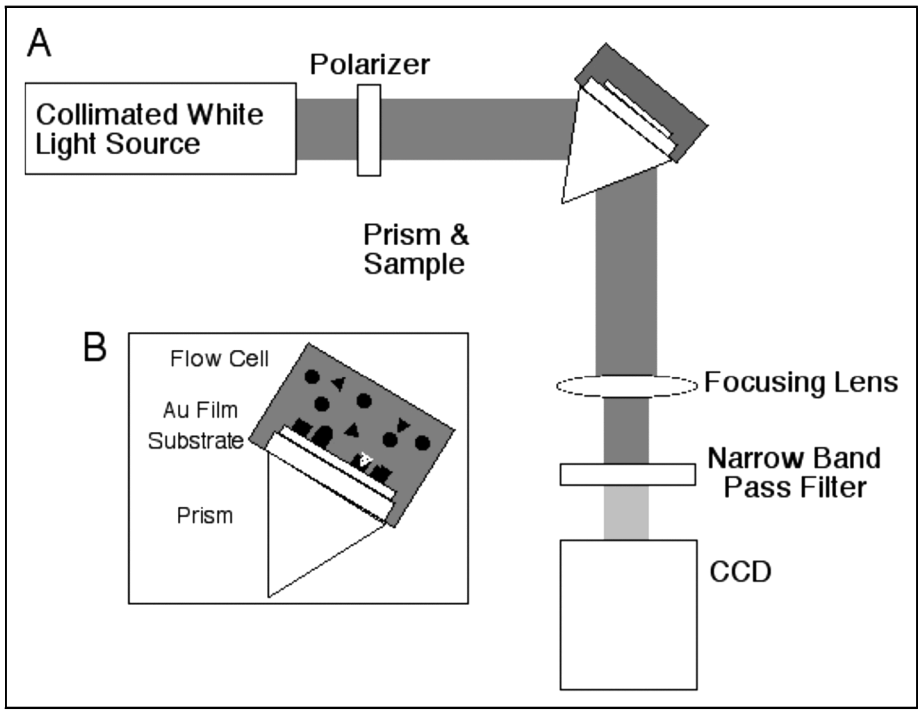

Fig. 4. **(A)** *A schematic diagram of an SPR imager: Collimated white light is passed through a polarizer and is incident on the sample assembly. Reflected light passes through focusing optics, a narrow band pass filter, typically centered at a wavelength in the near-infrared, and is captured by a CCD camera.* **(B)** *A schematic diagram of the sample assembly consisting of a glass prism that is optically coupled to a glass substrate containing a thin layer (45 nm) of gold. The sample is contained within a flow cell for in situ measurements.*

The deviations from linear behavior for $\Delta\%R$ and Δn_f are small provided that the experiment is performed at the optimal angle. If deviations are present they can be predicted and accounted for in the experimental results. As mentioned previously, the percent change in reflected light intensity due to the hybridization of a monolayer of 16-mer oligonucleotides is less than 1 percent, which falls within the region where linear data is obtained with SPR imaging.[9] An example of the use of SPR imaging to quantitate the amount of material adsorbing to a gold film is described in the Examples section. In this example the amount of protein adsorbing to a metal film is measured with SPR imaging and is used to construct adsorption isotherms for the interaction of proteins with immobilized carbohydrates.

EXAMPLES

Detection of DNA Hybridization: Single-Base Mismatch Detection in the Presence of Small Molecules. A recent example of the use of SPR imaging demonstrated that this technique can be used to monitor the hybridization of short oligonucleotides in the presence of small molecules that alter the oligonucleotide's binding properties.[27] A schematic diagram of a small molecule naphthyridine dimer that has been shown to stabilize the binding of G–G mismatches in double stranded DNA is shown in Fig. 6.[51–53] To demonstrate the G–G mismatch stabilizing properties of this molecule, a DNA array was fabricated using UV photopatterning. This involves a combination of self-assembly and UV photopatterning steps: A bare gold film is modified with a self-assembled monolayer of an amine-terminated alkanethiol. The amine-terminated surface is then reacted with a hydrophobic protecting group that can be reversibly removed from the surface. A quartz mask containing patterned features is placed over the modified gold film and the surface is exposed to UV light, resulting in the photooxidation of the gold–thiolate bond and generation of bare gold regions where the UV light is exposed to the surface. The substrate is then replaced in the amine-terminated alkanethiol solution, and a monolayer is formed at areas where there is bare gold. The resulting surface contains hydrophilic amine-terminated monolayer regions surrounded by a hydrophobic monolayer. The probe molecules can be immobilized through a series of reactions that are carried out within the hydrophilic wells by delivering small solution volumes to the surface (i.e., spotting solutions onto the surface with a pulled capillary). The hydrophobic background prevents cross-contamination between the array elements during the immobilization reaction. Once the probe compounds are immobilized on the surface, the hydrophobic protecting group is removed from the background. This generates an

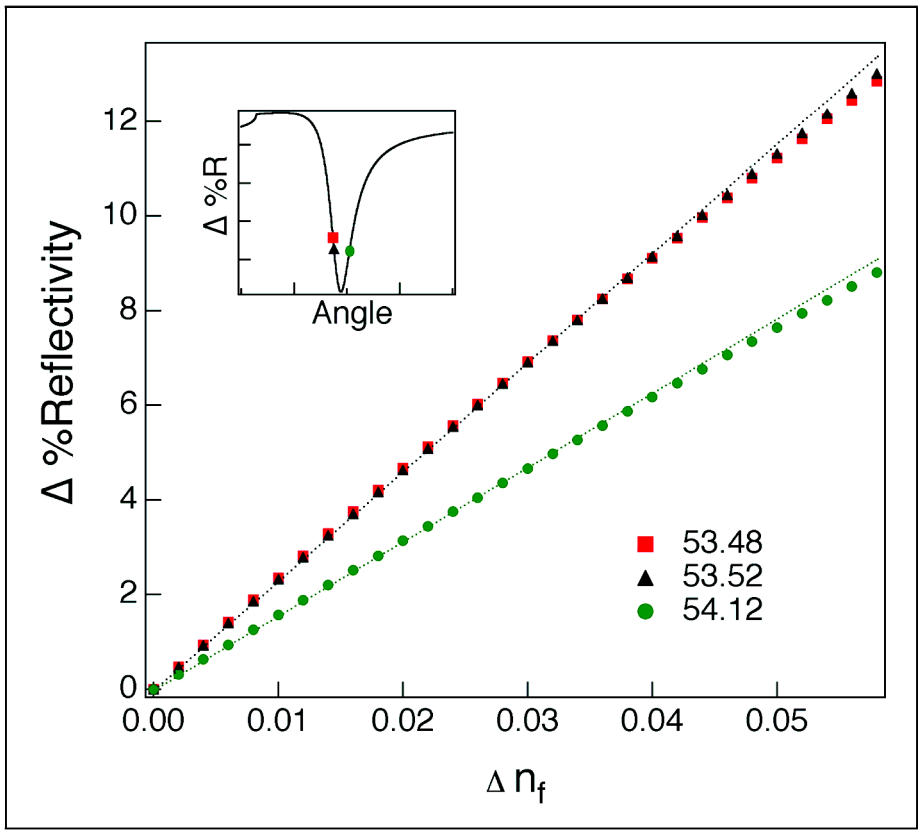

Fig. 5. Graph showing the absolute value of the change in percent reflectivity (%R) for the indicated change in the index of refraction (n_f) of the sensing layer. The data is plotted for three angles. The figure inset indicates the location of these points along the SPR curve. The data was obtained from 5-phase Fresnel calculations of the system shown in Fig. 2. The dotted lines correspond to linear relationships between Δ%R and Δn_f. Greater contrast is observed for larger values of Δ%R (i.e., at angles to the left of the plasmon angle).

amine-terminated background that is subsequently reacted with a molecule known to inhibit the adsorption of target compounds to the surface, such as the succinimide ester of polyethylene glycol.

To test the G–G mismatch stabilizing properties of the naphthyridine dimer shown in Fig. 6, a four-component DNA array was fabricated. Each of the four immobilized sequences in the array differed by one base. The position of this base is indicated by an X in sequence 1 (Fig. 7). The SPR difference image corresponding to the introduction of sequence 2 to the array shows that an SPR signal is only observed for the sequence containing the base cytosine (C) at the X position in sequence 1, the complementary sequence to sequence 2 (Fig. 7A). However, the SPR difference image corresponding to the addition of sequence 2 in the presence of the naphthyridine dimer shows that, in addition to its complement, sequence 2 also hybridizes to the sequence that forms a G–G mismatch. These results demonstrate that SPR imaging is a promising tool for monitoring single base mismatches in short oligonucleotides, and also demonstrates the possibility of using SPR imaging to screen molecules that alter the oligonucleotide's hybridization properties.

Protein Binding to Carbohydrate Arrays. Surface plasmon resonance imaging is an attractive tool for the study of proteins because there is no need to fluorescently, radioactively, or enzymatically label the analyte in order for it to be detected with SPR. This opens the possibility of directly studying an isolated protein with less sample processing and with less expense (i.e., the expense of the labeling reagents). It has been demonstrated that SPR imaging can be used to monitor protein adsorption onto DNA,[22] peptide,[54] and carbohydrate arrays.[55]

A recent example of the use of SPR imaging to study proteins is the study of protein–carbohydrate interactions.[55] It was shown that carbohydrate arrays could be fabricated using PDMS microchannels. A schematic diagram of this procedure is shown in Fig. 8. In this technique,[48] a three-dimensional silicon mask was used as a template to fabricate channels in the PDMS. These microchannels were composed of a series of parallel lines that had entrance and exit reservoirs at their ends for sample introduction. When the PDMS was placed over a modified

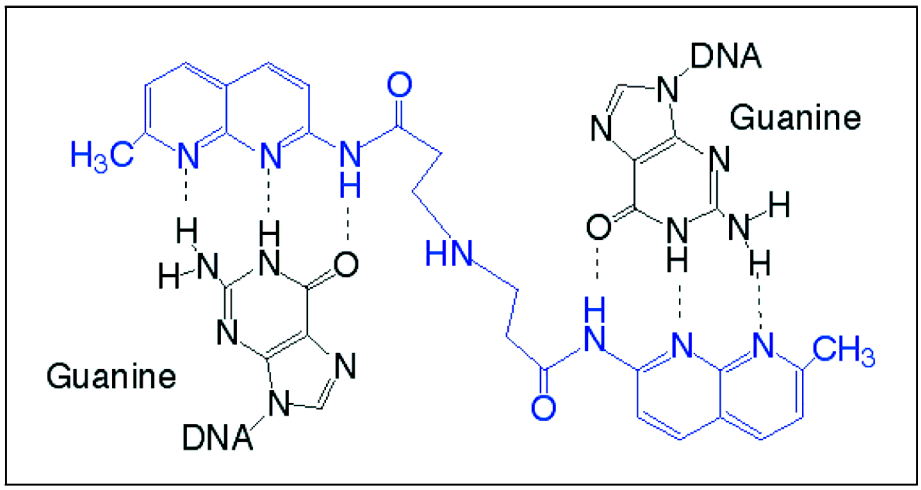

Fig. 6. Structure of the G–G mismatch stabilizing naphthyridine dimer that was used to generate the data shown in Fig. 7B. The naphthyridine dimer (blue) is shown hydrogen bonding to two guanine bases (black).

gold film, a different probe could be introduced and immobilized within each channel (Fig. 8, step A). Subsequent removal of the PDMS from the gold film yielded an array of probe molecules immobilized in a set of discrete lines (Fig. 8, step B).

A two-component carbohydrate array was used to monitor the adsorption of two carbohydrate binding proteins (lectins). A schematic diagram of the carbohydrate ligands is shown in Fig. 8. Compound 1 is a modified α–mannose ligand, and compound 2 is a modified α–galactose ligand. The two lectins studied were concanavalin A and jacalin. Concanavalin A has a known affinity for α–mannose and jacalin has a high affinity for α–galactose. Adsorption isotherms were constructed for the interactions of these lectins with the surface immobilized carbohydrates by monitoring the SPR imaging signal while increasing the concentration of the protein in solution. Shown in Fig. 9 are the adsorption isotherm for (squares) jacalin interacting with compound 2, and (circles) concanavalin A interacting with compound 1. Each data point was obtained by measuring the SPR imaging signal for the indicated protein concentration. Two examples of the SPR images used to construct the isotherms are shown in Fig. 9. The image on the left corresponds to the introduction of the lectin jacalin to the array, and the image on the right corresponds to the introduction of the lectin concanavalin A to the array.

The adsorption isotherms provide information about the interaction strength of the proteins with the carbohydrate surfaces. For example, the isotherms shown in Fig. 9 indicate that jacalin has a higher affinity for the immobilized α–galactose ligand than concanavalin A does for the α–mannose ligand. A number of possible applications for the use of SPR imaging to quantitate the interaction strength of proteins with immobilized arrays could be envisioned. These include the screening of compounds that might be of therapeutic significance, such as molecules that disrupt or enhance the interactions of proteins with DNA, proteins, or carbohydrates.

Antibody Binding to Protein Arrays. A recent example from the labs of Professors McDermott and Harrison at the University of Alberta demonstrates the use of SPR imaging to study the binding of antibodies to protein arrays.[56] The fabrication of the protein array utilized PDMS microchannels, as in the previous example, to pattern the surface of a gold film that had been modified with a carboxylic acid monolayer. Immobilization of the protein on the surface was carried out by flowing protein solutions through the PDMS microchannels. To image the arrays, the PDMS was removed from the surface and solutions of antibody were flowed over the array. Shown in Fig. 10 are the SPR images obtained by Kariuki and co-workers of a three-component protein array containing the proteins human fibrinogen (line 1), ovalbumin (line 2), and bovine IgG (line 3). Figure 10A shows the SPR difference image that was obtained after the array was exposed to the antibody for human fibrinogen, and Figs. 10B and 10C show the SPR difference images obtained after exposing the array to antibodies for anti-ovalbumin and anti-bovine IgG, respectively. These images show that there is a high degree of antibody binding specificity and a small degree of non-specific adsorption of the antibody to the array background, which the authors state could be improved upon further efforts to modify the array background. These results successfully demonstrate the suitability of using SPR imaging to study antibody binding to protein arrays and opens the possibility of using SPR imaging as a diagnostic tool for the study of antibodies.

CONCLUSION AND FUTURE DIRECTIONS

The label-free detection, high-throughput capabilities, and simple

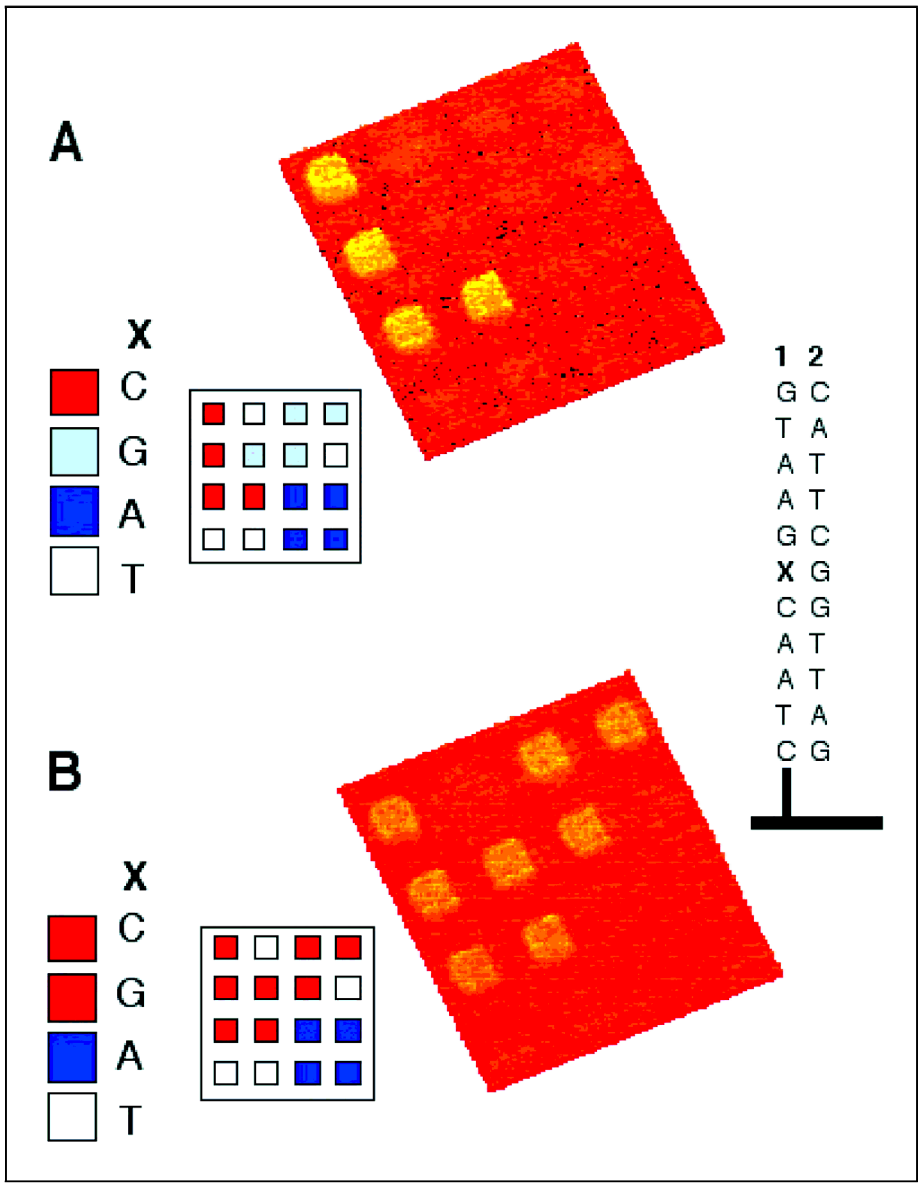

Fig. 7. SPR difference images of a four-component DNA array. Each immobilized oligonucleotide differs by one base, indicated by an X in sequence 1. The images were taken in the presence of (A) 1 μM sequence 2, or (B) 250 μM naphthyridine dimer with 1 μM sequence 1. The image shown in A indicates that sequence 2 only hybridizes to the perfect match. The image shown in B indicates that sequence 2 hybridizes to both the perfect match and the G–G mismatch oligonucleotide when naphthyridine dimer is present.

instrumental format make SPR imaging a useful tool for the study of a variety of biomolecular interactions. Examples of the use of SPR imaging to study biomolecular interactions have, thus far, been limited to arrays composed of 2–10 components; however, SPR imaging has the potential to screen arrays composed of at least 30 000 species on a 1.8 cm × 1.8 cm substrate.

It is expected that the high-throughput capabilities of SPR imaging will aid in the study of protein interactions, including protein–DNA, protein–peptide, protein–protein, and protein–cell surface interactions, in addition to those examples discussed in this article. There is, however, work that remains to be accomplished to make SPR imaging a routine detection method for the study of proteins. This includes the development of new array attachment methods, new array fabrication techniques, and improved analyte processing capabilities that more efficiently deliver solutions of target proteins to the array surface. Preliminary work has been done on the development of oriented arrays of fusion proteins for the study of protein–protein interactions with SPR

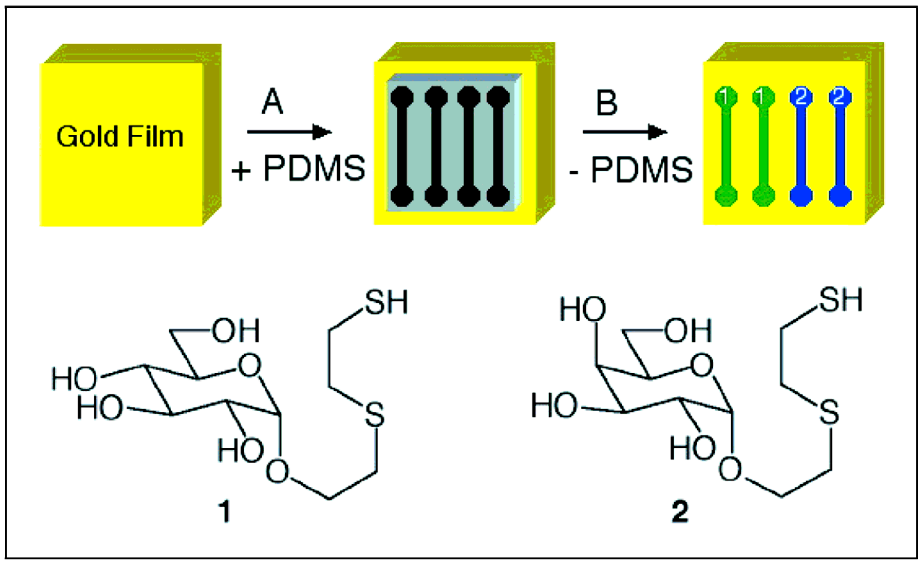

Fig. 8. Simplified schematic of the array fabrication process using polydimethylsiloxane microchannels. The microfabricated PDMS channels are placed on top of a modified gold film. Immobilization of the probe molecules occurs within the channels; upon removal of the PDMS from the surface, the probe ligands are immobilized in discrete lines on the gold film. A two-component array was fabricated to generate the data shown in Fig. 9. The two components are 1 *(a modified* α*–mannose ligand) and* 2 *(a modified* α*–galactose ligand).*

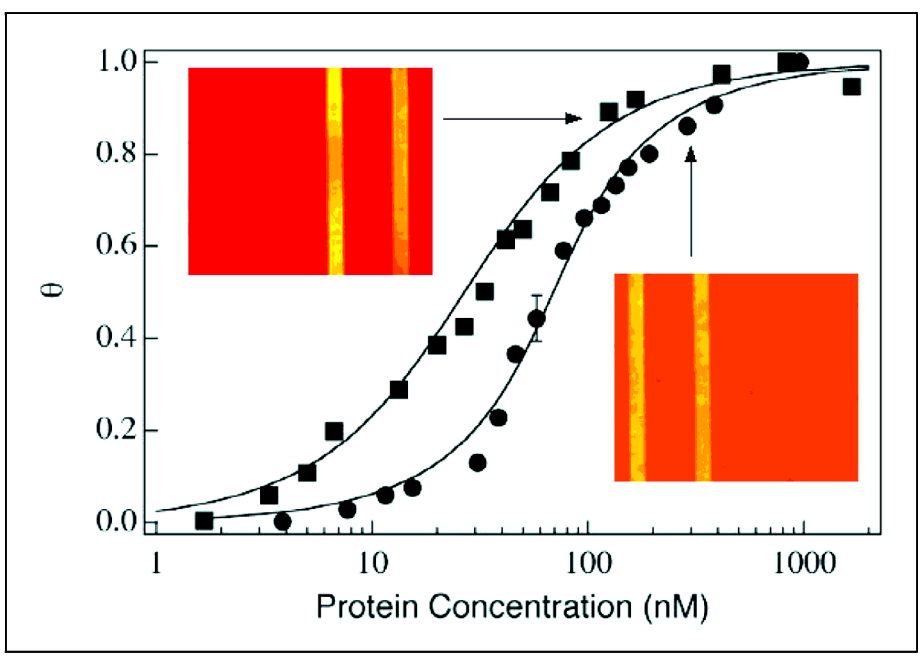

Fig. 9. Isotherms for (squares) the binding of jacalin to a surface containing compound 2 and (circles) the binding of concanavalin A to a surface containing compound 1. The relative protein surface coverage (fraction of occupied surface sites, θ*) was determined using SPR imaging as the concentration of protein in solution was increased. The data have been fit to Frumkin isotherms (solid lines), which provide information on the strength of the interaction between the surface immobilized species and the adsorbing species. The two SPR difference images are two-component carbohydrate arrays that were fabricated using the method shown in Fig. 8. The SPR image on the right shows the binding of the lectin concanavalin A to the mannose array elements, and the SPR image on the left shows the binding of the lectin jacalin to the galactose array elements. The images were used to generate two of the data points on the isotherms and to demonstrate the specificity of lectin binding to the immobilized carbohydrate ligands.*

imaging. This strategy uses a surface-based array of a capture agent to immobilize a set of fusion proteins that contain two domains: one invariant domain that binds to the capture agent and a second variable domain containing the probe protein, which is in direct contact with the target solution.

Finally, detection methods that increase the sensitivity of the SPR imaging technique will be extremely useful in a number of applications that require very low analyte concentrations, including environmental monitoring and DNA diagnostics. Increased sensitivity can currently be achieved through the use of labeled target molecules (i.e., latex, polystyrene, or gold nanoparticles conjugated to the target molecule) or through the use of a sandwich assay, in which the secondary binding event of a large molecule provides the detection signal.[20,25,57,58] These methods increase the complexity of the SPR imaging measurement. An alternate, promising method for achieving increased sensitivity in SPR imaging experiments is through improved instrumental design. One recent report demonstrated improved sensitivity with the technique of SPR interferometry, in which both the amplitude and phase of the reflected light are measured.[59–61] Near the surface plasmon angle there is a large shift in the phase of the reflected light. Measuring both the reflectivity and the phase of the light in an SPR imaging experiment may provide both an enhanced sensitivity and an increased dynamic range.

Other improvements in SPR imaging instrumentation are also in progress. For example, a portable, field-ready SPR imager is being developed for environmental monitoring, and the demonstration of Fourier transform SPR (FT-SPR) spectroscopy has expanded the use of SPR to near-infrared wavelengths (1000–2500 nm).[15] As a final note, it should be mentioned that SPR index of refraction measurements are just the simplest of many possible surface plasmon spectroscopies: SPR has also been used for SPR fluorescence,[62,63] SPR Raman scattering,[64] SPR CARS,[65] SPR electro-optical measurements,[66–68] and SPR second-harmonic generation at surfaces.[69]

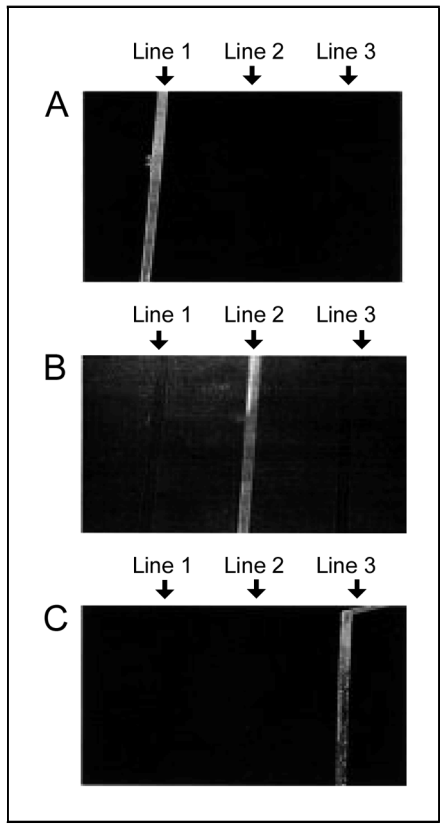

Fig. 10. SPR difference images of a three-component protein array containing the proteins human fibrinogen (line 1), ovalbumin (line 2), and bovine IgG (line 3). SPR difference images obtained after exposing the protein array to (A) the antibody to human fibrinogen; (B) the antibody to ovalbumin; and (C) the antibody to bovine IgG. Reproduced from Ref. 56 with kind permission from Kluwer Academic Publishing.

ACKNOWLEDGMENTS

This research is funded by the National Science Foundation (Grant CHE-0133151). The authors wish to thank Dr. Hye Jin Lee, Dr. Alastair Wark, Greta Wegner, and Berta Ostrander for their assistance in the preparation of the manuscript.

1. J. H. Watterson, P. A. E. Piunno, C. C. Wust, U. J. Krull, Sens. Actuators, B **74,** 27 (2001).
2. N. Sloper and M. T. Flanagan, Biosens. Bioelectron. **11,** 537 (1993).
3. F. S. Ligler, M. Breimer, J. P. Golden, D. A. Nivens, J. P. Dodson, T. M. Green, D. P. Haders, and O. A. Sadik, Anal. Chem. **74,** 713 (2002).
4. E. Garcia-Caurel, B. Drevillon, and A. L. S. De Martino, Appl. Opt. **44,** 7339 (2002).
5. T. Mutschler, B. Kiesser, R. Frank, and G. Gauglitz, Anal. Bioanal. Chem. **374,** 658 (2002).
6. L. Y. Li, S. F. Chen, S. J. Oh, and S. Y. Jiang, Anal. Chem. **74,** 6017 (2002).
7. J. Wang and A. J. Bard, Anal. Chem. **73,** 2229 (2001).
8. V. Silin and A. Plant, Trends Biotechnol. **15,** 353 (1997).
9. B. P. Nelson, T. E. Grimsrud, M. R. Liles, R. M. Goodman, and R. M. Corn, Anal. Chem. **73,** 1 (2001).
10. I. Gokce, E. M. Raggett, Q. Hong, R. Virden, A. Cooper, and J. H. Lakey, J. Mol. Biol. **304,** 621 (2000).
11. L. A. Lyon, M. D. Musick, and M. J. Natan, Anal. Chem. **70,** 5177 (1998).
12. R. Advincula, E. Aust, W. Meyer, and W. Knoll, Langmuir **12,** 3536 (1996).
13. D. G. Hanken, C. E. Jordan, B. L. Frey, and R. M. Corn, *Surface Plasmon Resonance Measurements of Ultrathin Organic Films at Electrode Surfaces* (Marcel Dekker, New York, 1996), vol. 20.
14. C. E. Jordan, B. L. Frey, F. R. Kornguth, and R. M. Corn, Langmuir **10,** 3642 (1994).
15. A. G. Frutos, S. C. Weibel, and R. M. Corn, Anal. Chem. **71,** 3935 (1999).
16. W. Hickel, D. Kamp, and W. Knoll, Nature (London) **339,** 186 (1989).
17. D. Piscevic, W. Knoll, and M. J. Tarlov, Supramol. Sci. **2,** 99 (1995).
18. B. Rothenhausler and W. Knoll, Nature (London) **332,** 615 (1988).
19. L. A. Lyon, W. D. Holliway, and M. J. Natan, Rev. Sci. Instrum. **70,** 2076 (1999).
20. C. E. Jordan, A. G. Frutos, A. J. Thiel, and R. M. Corn, Anal. Chem. **69,** 4939 (1997).
21. J. M. Brockman, B. P. Nelson, and R. M. Corn, Annu. Rev. Phys. Chem. **51,** 41 (2000).
22. E. A. Smith, M. G. Erickson, A. T. Ulijasz, B. Weisblum, and R. M. Corn, Langmuir **19,** 1486 (2003).
23. www.biacore.com.
24. D. Piscevic, R. Lawall, M. Veith, M. Liley, Y. Okahata, and W. Knoll, Appl. Surf. Sci. **90,** 425 (1995).
25. L. He, M. D. Musick, S. R. Nicewarner, F. G. Salinas, S. J. Benkovic, M. J. Natan, and C. D. Keating, J. Am. Chem. Soc. **122,** 9071 (2000).
26. M. Li, H. J. Lee, A. E. Condon, and R. M. Corn, Langmuir **18,** 805 (2002).
27. E. A. Smith, M. Kyo, H. Kumasawa, K. Nakatani, I. Saito, and R. M. Corn, J. Am. Chem. Soc. **124,** 6810 (2002).
28. H. Raether, *Surface Plasmons on Smooth and Rough Surfaces and on Gratings* (Springer-Verlag, Berlin, 1988).
29. P. B. Johnson and R. W. Christy, Phys. Rev. B **6,** 4370 (1972).

30. E. Kretschmann and H. Raether, Z. Naturforsch., A: Phys. Sci. **23,** 2135 (1968).
31. W. N. Hansen, J. Opt. Soc. Am. **58,** 380 (1968).
32. B. P. Nelson, A. G. Frutos, J. M. Brockman, and R. M. Corn, Anal. Chem. **71,** 3928 (1999).
33. H. E. de Bruijin, R. P. H. Kooyman, and J. Greve, Appl. Opt. **32,** 2426 (1993).
34. C. E. H. Berger, R. P. H. Kooyman, and J. Greve, Rev. Sci. Instrum. **65,** 2829 (1994).
35. T. M. Herne and M. J. Tarlov, J. Am. Chem. Soc. **119,** 8916 (1997).
36. B. L. Frey and R. M. Corn, Anal. Chem. **68,** 3187 (1996).
37. K. L. Prime and G. M. Whitesides, J. Am. Chem. Soc. **115,** 10714 (1993).
38. J. Lahiri, L. Isaacs, B. Grzybowski, J. D. Carbeck, and G. M. Whitesides, Langmuir **15,** 7186 (1999).
39. B. T. Houseman and M. Mrksich, Angew. Chem., Int. Ed. Engl. **38,** 782 (1999).
40. A. G. Frutos, J. M. Brockman, and R. M. Corn, Langmuir **16,** 2192 (2000).
41. J. M. Brockman, A. G. Frutos, and R. M. Corn, J. Am. Chem. Soc. **121,** 8044 (1999).
42. C. D. Bain and G. M. Whitesides, J. Am. Chem. Soc. **110,** 3665 (1988).
43. C. D. Bain and G. M. Whitesides, Science (Washington, D.C.) **240,** 62 (1988).
44. R. G. Chapman, E. Ostuni, L. Yan, and G. M. Whitesides, Langmuir **16,** 6927 (2000).
45. R. G. Chapman, E. Ostuni, S. Takayama, R. E. Holmlin, L. Yan, and G. M. Whitesides, J. Am. Chem. Soc. **122,** 8303 (2000).
46. E. Ostuni, R. G. Chapman, R. E. Holmlin, S. Takayama, and G. M. Whitesides, Langmuir **17,** 5605 (2001).
47. C. D. Bain, E. B. Troughton, Y. T. Tao, J. Everall, G. M. Whitesides, and R. G. Nuzzo, J. Am. Chem. Soc. **111,** 321 (1989).
48. H. Lee, T. T. Goodrich, and R. M. Corn, Anal. Chem. **73,** 5525 (2001).
49. A. T. A. Jenkins, T. Neumann, and A. Offenhausser, Langmuir **17,** 265 (2001).
50. M. Zizlsperger and W. Knoll, Prog. Colloid Polym. Sci. **109,** 244 (1998).
51. K. Nakatani, S. Sando, and I. Saito, Bioorg. Med. Chem. **9,** 2381 (2001).
52. K. Nakatani, S. Sando, H. Kumasawa, J. Kikucji, and I. Saito, J. Am. Chem. Soc. **123,** 12650 (2001).
53. K. Nakatani, S. Sando, and I. Saito, Nat. Biotech. **19,** 51 (2001).
54. G. J. Wegner, H. J. Lee, and R. M. Corn, Anal. Chem. **74,** 5161 (2002).
55. E. A. Smith, W. D. Thomas, L. L. Kiessling, and R. M. Corn, J. Am. Chem. Soc. **125,** 6140 (2003).
56. J. K. Kariuki, V. Kanda, M. T. McDermott, and D. J. Harrison, in *Micro Total Analysis Systems 2002,* Y. Baba, S. Shoji, and A. van der Berg, Eds. (Kluwer Academic Publisher, Nara, Japan, 2002), vol. 1, pp. 230–232.
57. T. Wink, S. J. van Zuiken, A. Bult, and W. P. van Bennekom, Anal. Chem. **70,** 827 (1998).
58. J. H. Gu, H. Lu, Y. W. Chen, L. Y. Liu, P. Wang, J. M. Ma, and Z. H. Lu, Supramol. Sci. **5,** 695 (1998).
59. P. I. Nikitin, A. A. Beloglazov, V. E. Kochergin, M. V. Valeiko, and T. I. Ksenevich, Sens. Actuators, B **54,** 43 (1999).
60. A. N. Grigorenko, P. I. Nikitin, and A. V. Kabashin, Appl. Phys. Lett. **75,** 3917 (1999).
61. A. V. Kabashin and P. I. Nikitin, Opt. Commun. **150,** 5 (1998).
62. S. Roy, J.-H. Kim, J. T. Kellis, A. J. Poulose, C. R. Robertson, and A. P. Gast, Langmuir **18,** 6319 (2002).
63. T. Liebermann and W. Knoll, Langmuir **19,** 1567 (2003).
64. R. M. Corn and M. R. Philpott, J. Phys. Chem. **80,** 5245 (1984).
65. C. K. Chen, A. R. D. De Castro, Y. R. Shen, and F. DeMartini, Phys. Rev. Lett. **43,** 946 (1979).
66. D. G. Hanken, R. R. Naujok, J. M. Gray, and R. M. Corn, Anal. Chem. **69,** 240 (1997).
67. D. G. Hanken and R. M. Corn, Anal. Chem. **69,** 3665 (1997).
68. C. Xia, R. Advincula, A. Baba, and W. Knoll, Langmuir **18,** 3555 (2002).
69. R. M. Corn, M. Romagnoli, M. D. Levenson, and M. R. Philpott, J. Phys. Chem. **81,** 4127 (1984).